Recovering Higher Order Modes in the Ringdown of Binary Black Hole Coalescences

Rachel Mechum*
University of Florida

Mentors: Richard Udall† and Alan Weinstein‡
California Institute of Technology
LIGO Laboratory, Caltech
(Dated: September 15, 2022)

Disturbances in the curvature of spacetime from the coalescence of binary black holes can be probed by the gravitational radiation emitted by these sources and recorded by Advanced LIGO and Virgo. The merger of such objects allows us to test Einstein's theory of general relativity in the regime of strong and highly dynamical gravity - specifically, the newly formed black hole rings down in a series of quasinormal modes, whose frequencies and damping rates are fully predicted by general relativity. We focus on the ringdown of the remnant black hole, implementing ringdown analysis in the time domain. We demonstrate the ability to fit and recover higher order modes of the ringdown within a set of simulated IMR signals. Possible deviations of the frequencies and damping times of the ringdown may point to new physics beyond general relativity, such as quantum gravity that we are not yet familiar with.

Keywords: gravitational waves, general relativity, LIGO, quasinormal modes, compact binary mergers

I. MOTIVATION

Gravitational wave (GW) signals from compact binary coalescences (CBC) of binary black holes (BBH) provide crucial information to understand what remains of the remnant black hole (BH) and allow us to test general relativity (GR) in the regime of strong and highly dynamical gravity.

GW signals are detected by the Laser Interferometer Gravitational-wave Observatory (LIGO) [1]. LIGO consists of two detectors that are 3,000 kilometers apart. LIGO exploits the physical properties of light and of space itself to detect and understand the origins of GWs [2].

Binary neutron stars (BNS), black hole-neutron star (BHNS), and BBHs are the three main classes of detectable CBCs from our current ground-based detectors. Future detectors such as LISA will allow us to study more types of CBCs. The data from BBH mergers come from real events [1], but are simulated to better understand our current models and refine our analysis techniques.

During a BBH coalescence, there are 3 stages: the inspiral, merger, and ringdown (IMR). The remnant of merged BHs is a single perturbed BH with a GW waveform characterized as a set of complex frequencies and damping times known as quasinormal modes (QNMs), which are unambiguously predicted by GR. The gravitational radiation from this remnant is called the ringdown phase [3].

BH ringdown is an effective probe of GR in the strong field, notably the "no-hair theorem" (NHT) [4]. Detections of deviations from GR in the form of violations of NHT can point to physics beyond GR [5]. We model the ringdown (not to be confused with the "ringdown phase" of IMR mentioned above) to be a linear superposition of damped sinusoids,

$$\sum_{lmn} A_{lmn} e^{-t/\tau_{lmn}} sin(2\pi f_{lmn} t + \phi_{lmn}), \tag{1}$$

where l and m index the angular modes, n is the overtone, A is the amplitude of the waveform, τ is the damping time, f is the frequency, and ϕ is the phase (see FIG.1). Compactly, the ringdown is a set of complex frequencies, ω,

$$\omega = 2\pi f + i/\tau, \tag{2}$$

determined by the nature of the remnant BH [6].

The dominant quasinormal mode in GR is recognized as 220, where $l = m = 2$ and $n = 0$. This mode displays the highest frequency and is the least damped, which we label as the fundamental 22 mode. Higher order modes (HOMs) of QNMs are the modes with smaller amplitudes than the dominant 22 mode: 330, ... , 440.

HOMs that have a radial mode $n > 0$ are referred to as overtones. Overtones are the QNMs with faster damping times than $n = 0$ [7]. In previous data analysis, the inclusion of overtones was omitted which led to loss of signal content. That is to say, the inclusion of overtones is important to increase the detection SNR and extract the parameters of the signal more accurately [5] and further the field of BH spectroscopy.

In GR, the GW ringdown frequencies and damping times reveal the final mass and spin of the merged BH. The frequencies for a Kerr BH do not depend upon its dynamical past, but the amplitudes of the ringdown do. This leads to the discussion of the NHT. The NHT states that mass and spin are the only two properties of Kerr BHs in GR. Therefore, they uniquely determine each

* rachel.mechum@ufl.edu
† rudall@caltech.edu
‡ ajw@caltech.edu

f_{lmn} and τ_{lmn}. We can test the NHT with the data collected during previous and future runs of GW detectors [7].

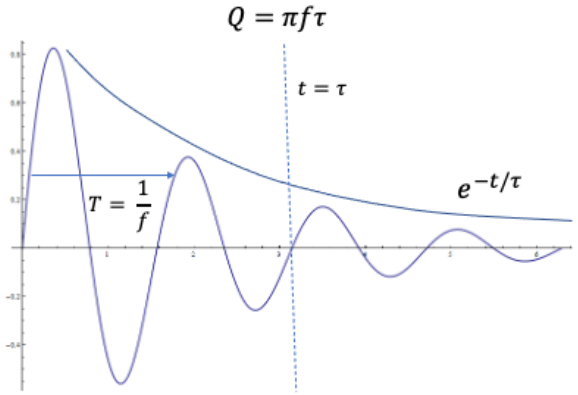

FIG. 1. Example of a single damped sinusoidal QNM. T is the period, Q is the quality factor, and $e^{-t/\tau}$ is the exponential decay. By setting $t = \tau$, we can see the quality factor for the QNM illustrated here will be ~ 2. When adding multiple QNMs, the equation will result in a linear superposition of damped sinusoidal oscillations, as seen in Eqn.1.

II. APPROACH AND METHODS

Recovering higher order QNMs is a powerful way to test Einstein's theory of GR. This proves to be more difficult once passing the dominant angular mode 22. In this analysis, we will simulate real GW signals in the time domain. By using the time domain, we can adjust the start time of the ringdown to produce better results for recovery of HOMs.

The framework for this research is based on work done by Maximiliano Isi and Will Farr [8], who analyzed ringdowns not in the frequency domain, but in the time domain. However, this approach demands truncating the GW signal at a specific time, which is difficult to handle with the usual LIGO-Virgo analysis techniques. Instead, it calls for special treatment in the time domain, or an equivalent nontrivial procedure in the frequency domain [7–11]. We chose to work with the former and use the *RINGDOWN* software package [8, 12].

A. QNM Properties

Before getting into the recovery of HOMs from BBH coalescences, we first need to understand how HOMs and overtones behave. This way, we can be confident in our understanding when we analyze them in the ringdown.

Referencing to a paper by Isi and Farr [8], we start by recreating a plot for dimensionless frequencies, dimensionless damping times, and quality factor as a function of dimensionless BH spin. The frequencies and damping times are dimensionless due to the variable t_M, a time constant associated with BH mass and is expressed as,

$$t_M = \frac{GM}{c^3} \tag{3}$$

where G is the gravitational constant, M is the mass, and c is the speed of light. Instead of focusing on the dominant 22 mode, we dive deeper into other subdominant modes (see FIGs.2-4).

One major point to make is when increasing the angular modes, the frequency increases. The overtones of each mode all reveal the zeroth overtone to be the most dominant, with the greatest values for frequencies, damping times, and quality factor. The other overtones fall beneath the threshold of the zeroth overtone's value. The damping times and quality factor don't seem to change significantly, but there is a small change between modes.

1. *Complex Frequencies and Damping Times*

As previously stated, all QNMs have their own distinct frequencies and damping times that are derived directly from the mass and spin of the remnant BH. With these frequencies and damping times, we can plot them against respective values of χ ranging from 0-1 (see FIGs.2-4).

Analyzing the plots, we can see that with increasing multipoles, their frequency and Q factor is climbing. We can also note that in each leftmost plot, the frequencies of each overtone are spread at $\chi = 0$. The frequencies and damping times diverge towards infinity at $\chi = 1$, but never reach due to the extremal spins of astrophysical BHs ($\chi < 1$).

2. *Dominant Mode and Overtones*

When analyzing the fundamental 220 mode, we understand why this is labeled the dominant mode. This mode can be more easily recovered due to how 'loud' (highest amplitude A in Eqn.1) it is compared to subdominant modes. Berti et al. [13] showed that the ringdown analysis with only the 220 mode can lose 10% of potential LIGO events [3]. Since this fundamental mode behaves just as we expect (by having the highest frequency in the 22 mode and showing to be the least damped), this makes it the best recovery target.

When adding overtones, the frequencies and damping times of the wave decreases as can be seen in FIGs.2-4. Recovering ringdowns with higher overtones is where the task becomes more difficult. For us to efficiently be able to recover the 22 mode and higher overtones, we would need a louder event or a more sensitive detector.

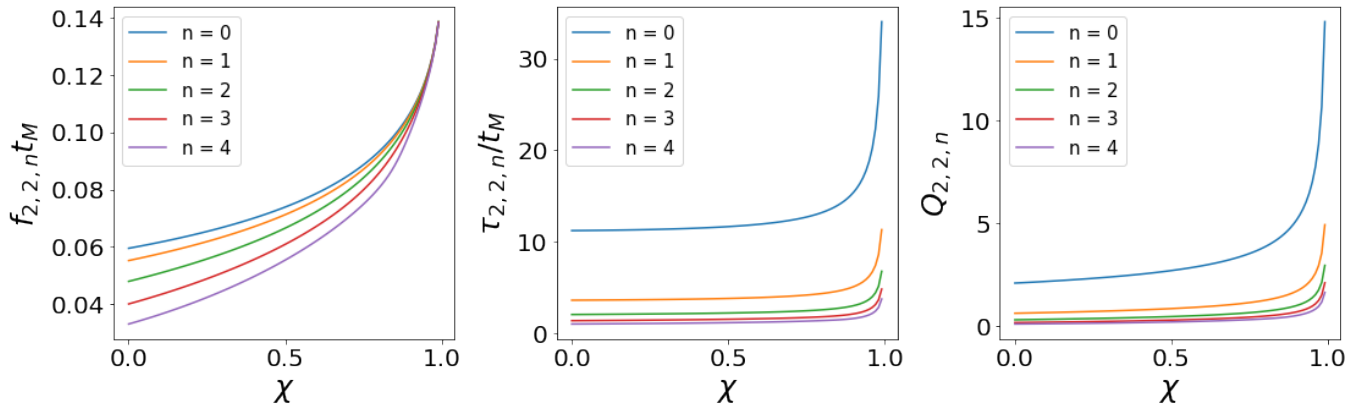

FIG. 2. Dimensionless frequency f_{22n} (left), dimensionless damping time τ_{22n} (center) and quality factor $Q_{22n} = \pi f_{22n}\tau_{22n}$ (right) for changing $l = m = 2$ tones, as a function of dimensionless BH spin χ. Times are measured in units of $t_M \equiv GM/c^3$ for BH mass M.

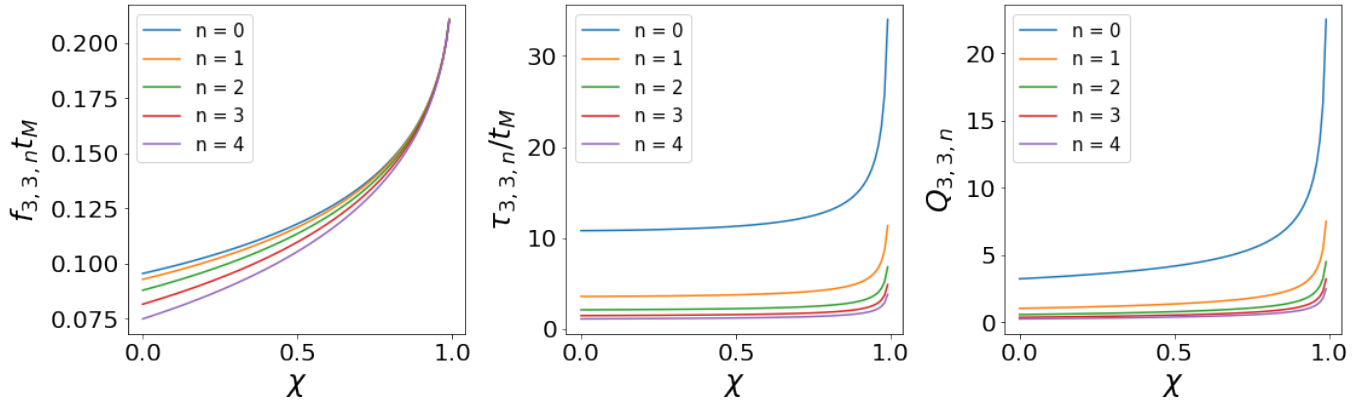

FIG. 3. Dimensionless frequency f_{33n} (left), dimensionless damping time τ_{33n} (center) and quality factor $Q_{33n} = \pi f_{33n}\tau_{33n}$ (right) for changing $l = m = 3$ tones, as a function of dimensionless BH spin χ.

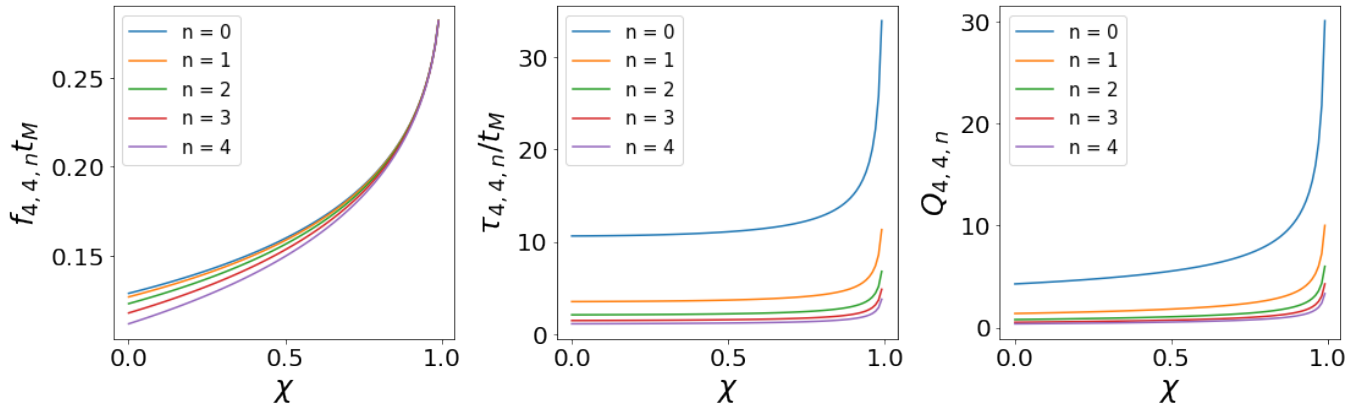

FIG. 4. Dimensionless frequency f_{44n} (left), dimensionless damping time τ_{44n} (center) and quality factor $Q_{44n} = \pi f_{44n}\tau_{44n}$ (right) for changing $l = m = 4$ tones, as a function of dimensionless BH spin χ.

3. Subdominant Modes and Overtones

Simulating the subdominant modes along with their overtones is imperative to understand how to deconstruct real waveforms. When we begin recovering these HOMs in true ringdown data, we will know what to search for and soon be confident in what and where the best events are to spot them.

Beginning with the first subdominant angular mode ($l = m = 3, n = 0$), we note an increase in frequency from the dominant fundamental mode ($l = m = 2, n = 0$). The subdominant mode 33 is consistent in the decrease in frequency with increasing overtones. We see the same information when simulating the ($l = m = 4$) fundamental mode along with various overtones.

B. Waveform Fitting

Waveform fitting is crucial in the process of recovering QNMs. We use our knowledge of QNMs to create an algorithm that fits to a specific waveform's properties.

For these simulated post-merger events, we are able to specify the angular modes, l and m, as well as the overtone, n. In return, we have access to the frequencies and damping times of different modes and overtones [14]. The amplitude, phase, frequencies, and damping times are all accounted for in the fitting process. The fitting algorithm itself fits for the amplitudes and phases of each individual mode and the remnant mass and spin.

To start waveform fitting, we begin with a noiseless IMR signal. We use PyCBC [15] waveform generators and approximants IMRPhenomXP (XP) [16] and IMRPhenomXPHM (XPHM) [16]. Both of these approximants are useful to create phenomenological inspiral, merger, and ringdown waveforms for multiple cases of merging BHs. XP accounts for the 22 mode and a number of overtones while XPHM accounts for the 21,22,32,33, and 44 modes and overtones. XP is simply a portion of XPHM.

By supplying these approximants with a luminosity distance, inclination angle, mass and spin for each BH in the system, they will generate waveforms on a case-by-case basis. Here, the inclination angle is the angle between our line of site to the source and the orbital angular momentum direction, normal to the binary orbital plane. An inclination angle of 0 corresponds to a binary orbit that is "face-on" and $\pi/2$ is an "edge-on" orbit.

We chose to work with three cases: equal masses and no spins, equal masses and z-component only spins, unequal masses and no spins. Each case is tested in both of the waveform approximants used in our analysis, XP and XPHM.

To be sure that our fitting algorithm returns accurate values for remnant mass and spin, amplitude, and phase of each QNM, we implement the use of another Python package, surfinBH [17, 18]. By giving surfinBH a mass ratio and spin magnitudes, it generates a value of expected remnant BH mass and spin with a 1-σ error estimate. We compare these to our remnant values from the waveform fit to see how well they compare and if our values are acceptable according to surfinBH (see Table I).

An additional check for goodness-of-fit was calculating residual values. The residual value we calculate is as follows,

$$1 - R^2 = \frac{SS_{res}}{SS_{tot}}, \tag{4}$$

where SS_{res} is the sum of squares of the residual (the addition of the squares of deviations from actual values of data) and SS_{tot} is the total sum of squares (the sum over all differences from calculated data and overall mean squared). For the best $1 - R^2$ value, the residual sum of squares variable needs to be small (close to zero) so when divided by the larger value of the total sum of squares, the value remains small - a well-fit waveform.

III. RESULTS

In this section, we discuss differences between the XP and XPHM waveform approximant. By evaluating three different cases, we focus mainly on how t_0, the start time of the ringdown to be analyzed, can be shifted to reflect a smaller $1 - R^2$ value and exhibit the inclination dependency of that value. For the non-precessing systems that we are considering here, the inclination angle is constant throughout the inspiral and merger and the resulting remnant BH spin is aligned with binary orbital angular momentum. The higher order mode content of the GW is known to be a strong function of that inclination angle.

To achieve an acceptable $1 - R^2$ value, we first had to test what could possibly affect the fit. One major factor (noted in Isi and Farr [8]) was that ringdown analysis can be highly affected by what time we decide to signal the start of the ringdown. To account for this, we generated waveforms and fits at multiple different start times to see how the goodness-of-fit would alter.

A. IMRPhenomXP

In XP, there was a successful recovery of the 22 mode along with its overtones n=0,1,2. By allowing the algorithm to recover 220, 221, and 222 values for amplitude, phase, along with remnant mass and spin, we present an acceptable fit of a generated BBH merger waveform (see FIG.5).

When calculating the $1 - R^2$ value at every t_0 and individual inclination, the data reveals where the best fit will occur. As shown in FIG.6, we see how the plots and data change with different cases. The earlier and later times show high values of $1 - R^2$, then there is a noticeable centrally located dip where we have the best values.

For inclinations considered, we see that a ringdown start time of $t_0 = 1ms$ results in a better fit than for $t_0 = 0s$. We note a strong inclination dependence for these XP cases. The majority of this dependence happens when $t_0 > 0$, inclinations showing separation after 0s.

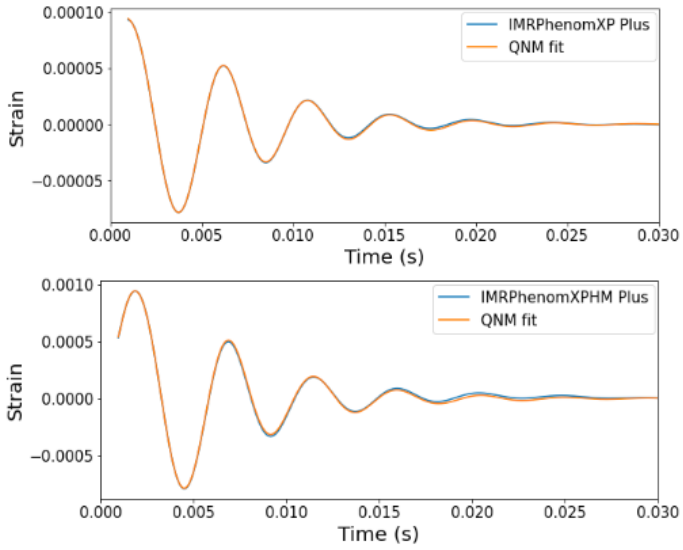

FIG. 5. Waveform fits for specific case of equal masses and no spins with an inclination angle of 0 and $t_0 = 0.001s$. Top plot is XP approximant and bottom plot is XPHM.

QNM Fit Remnant Mass $M_f(M_\odot)$	**SurfinBH** Remnant Mass $M_f(M_\odot)$	Error %
76.1 $[t_0 = 00.00s]$	76	0.13
78.0 $[t_0 = 00.01s]$	76	2.63
78.2 $[t_0 = 00.02s]$	76	2.89
77.9 $[t_0 = 00.03s]$	76	2.50
77.9 $[t_0 = 00.04s]$	76	2.50
...	...	...

QNM Fit Remnant Spin χ_f	**SurfinBH** Remnant Spin χ_f	Error %
0.66 $[t_0 = 00.00s]$	0.69	4.35
0.71 $[t_0 = 00.01s]$	0.69	2.90
0.71 $[t_0 = 00.02s]$	0.69	2.90
0.69 $[t_0 = 00.03s]$	0.69	0.00
0.69 $[t_0 = 00.04s]$	0.69	0.00
...	...	...

TABLE I. SurfinBH versus QNM Fit parameter estimation results. The changing row values in each column represent an estimated remnant mass and spin. In this table, the values of the QNM Fit column are based on an XPHM equal masses and no spin case where the inclination angle is 0 and t_0 ranges from 0.00s-0.004s.

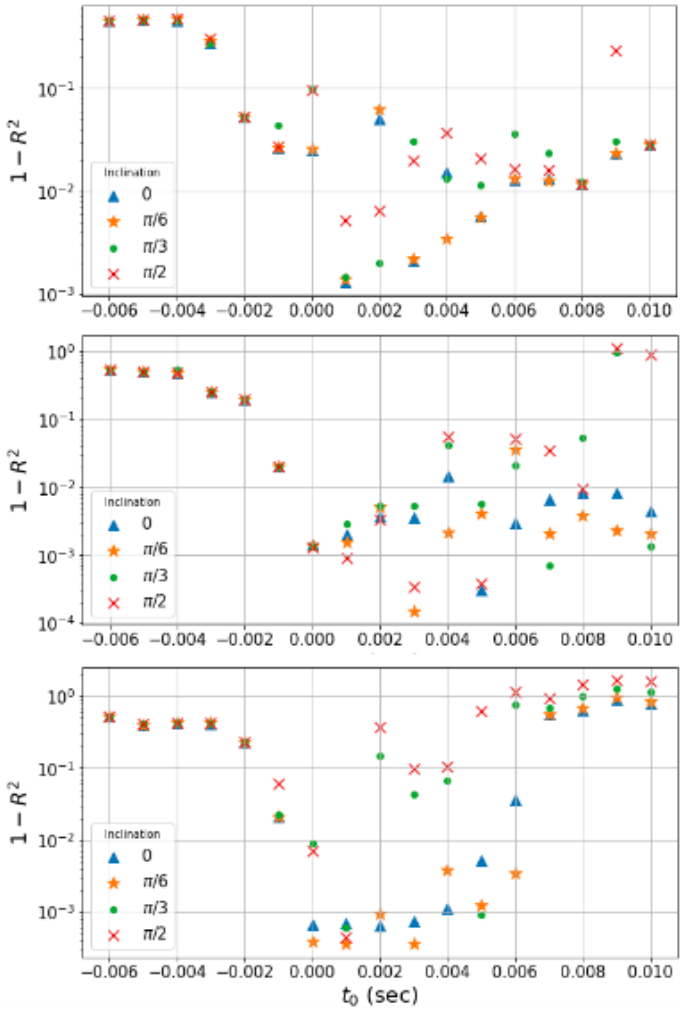

FIG. 6. XP's inclination dependence at different start times of the ringdown analysis. Uppermost plot is an equal mass ($M_1 = M_2 = 40M_\odot$) case with all spins set to zero. Middle plot is an equal mass case but with spins of each BH set to 0.5 in the z-direction. Bottom plot is showing an unequal mass ($M_1 = 40M_\odot$, $M_2 = 20M_\odot$) case with all spins set to zero. The best fits in all plots happen around the $t_0 = 0$ time with the far left and right data points showing high values of $1 - R^2$. The remnant mass, M_f, for the equal mass cases is estimated to be $76M_\odot$ where $t_M = .0004s$. For unequal mass case, M_f is estimated at $58M_\odot$ where $t_M = .0003s$.

B. IMRPhenomXPHM

For the XPHM approximant, there was also a successful recovery of the modes included. These modes being 21,22,32,33, and 44 along with their zeroth, first, and second overtones. The algorithm has fit for every mode configuration's amplitude, phase, remnant mass, and remnant spin of the final BH.

In FIG.7, the plots also present the $1-R^2$ value at each t_0 with an inclination dependency. Here we see that, at least for the case of equal masses in the binary, the best fit is obtained when t_0 is slightly negative. There isn't as

drastic of a slope when starting at earlier times as there is with XP. As we mover farther away from $t_0 = 0$ ringdown start time, the values of $1 - R^2$ become gradually worse.

There is also a weak dependence on inclination angle. The four different inclination angle values all stay relatively close to one another as the start time changes.

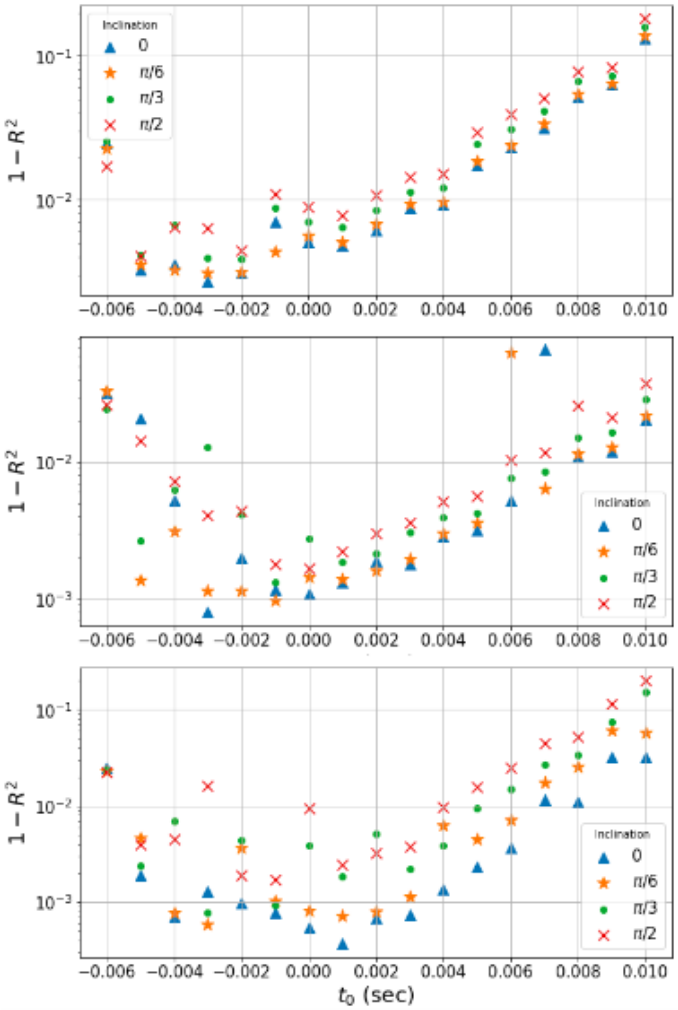

FIG. 7. XPHM's inclination dependence at different start times of the ringdown analysis. Uppermost plot is an equal mass ($M_1 = M_2 = 40M_\odot$) case with all spins set to zero. Middle plot is an equal mass case but with spins of each BH set to 0.5 in the z-direction. Bottom plot is showing an unequal mass ($M_1 = 40M_\odot$, $M_2 = 20M_\odot$) case with all spins set to zero. The best fits for the top plot happens to appear in the merger time, before $t_0 = 0$. The best fits in the middle and bottom plots are centered at the $t_0 = 0$ time with the far left and right data points showing greater values of $1 - R^2$. The remnant mass, M_f, for the equal mass cases is estimated to be $76M_\odot$ where $t_M = .0004s$. For unequal mass case, M_f is estimated at $58M_\odot$ where $t_M = .0003s$.

IV. FUTURE WORK

There is still much to be researched within BH spectroscopy. What this paper has proven is that we are fully confident in recovering multiple higher order QNMs with different cases of BBH coalescences.

One step that would be extremely beneficial for a continued analysis is adding simulated noise on top of the GW signal. By doing this, we would introduce new techniques and further our understanding for future real signals. Adding more system cases is also a topic of interest. With case expansion, we will have more reliable information and a better grasp on what we will possibly see and recover in the future.

The final step for this work would be to use this analysis on real GW signals. This would be a true test of our recovery of QNMs from a noise-filled signal along with a test of the NHT and gravity in the strong regime.

V. CONCLUSION

Higher order QNMs from BBH mergers have proven to be extremely significant in the ringdown phase of the GW signal. Here, we have expressed how QNMs help to describe properties of the remnant BH and the HOMs allow us to test GR in the strong regime.

We have shown only noiseless scenarios, but the data from these noiseless signals are useful. By showcasing that the start time of the ringdown phase is a large factor in goodness-of-fit and recovery, this is a functional part of past, current, and future ringdown analysis. On top of this, inclination dependency is also to take note of. With approximant XP, inclination dependency was high due to attempting to recover only one mode with a few overtones. When using XPHM approximant with additional modes and their overtones, we see a much weaker dependence on inclination angle.

The future of HOM recovery within the ringdown of BBH systems is promising. With many people working on problems similar to the one presented in this paper, there will be more information available about these processes in the near future. We are hopeful to uncover more about QNMs of BH mergers and how they will present themselves in the future with even more sensitive detectors.

ACKNOWLEDGMENTS

I wish to acknowledge the tremendous support of my mentors, Richard Udall and Alan Weinstein, for offering suggestions and encouragement to help further my research. I also gratefully recognize the support from the National Science Foundation Research Experience for Undergraduates (NSF REU) program, the California Institute of Technology, and the LIGO Laboratory Summer Undergraduate Research Fellowship.

[1] The LIGO Scientific Collaboration and the Virgo Collaboration, B. Abbott et al., *GWTC-3: Compact Binary Coalescences Observed by LIGO and Virgo During the Second Part of the Third Observing Run*, arXiv e-prints , arXiv:2111.03606 (2021), arXiv:2111.03606 [gr-qc].

[2] *What is LIGO?*

[3] N. Sago, S. Isoyama, and H. Nakano, *Fundamental Tone and Overtones of Quasinormal Modes in Ringdown Gravitational Waves: A Detailed Study in Black Hole Perturbation*, Universe **7**, 357 (2021).

[4] J. D. Bekenstein, *Novel "no-scalar-hair" theorem for black holes*, Phys. Rev. D **51**, R6608 (1995).

[5] X. Forteza, S. Bhagwat, P. Pani, and V. Ferrari, *Spectroscopy of binary black hole ringdown using overtones and angular modes*, Physical Review D **102** (2020).

[6] R. Brito, A. Buonanno, and V. Raymond, *Black-hole spectroscopy by making full use of gravitational-wave modeling*, Physical Review D **98**, 10.1103/physrevd.98.084038 (2018).

[7] M. Isi, M. Giesler, W. M. Farr, M. A. Scheel, and S. A. Teukolsky, *Testing the No-Hair Theorem with GW150914*, Physical Review Letters **123**, 10.1103/physrevlett.123.111102 (2019).

[8] M. Isi and W. M. Farr, *Analyzing black-hole ringdowns* (2021).

[9] J. Veitch, V. Raymond, B. Farr, W. Farr, P. Graff, S. Vitale, B. Aylott, K. Blackburn, N. Christensen, M. Coughlin, W. D. Pozzo, F. Feroz, J. Gair, C.-J. Haster, V. Kalogera, T. Littenberg, I. Mandel, R. O'Shaughnessy, M. Pitkin, C. Rodriguez, C. Röver, T. Sidery, R. Smith, M. V. D. Sluys, A. Vecchio, W. Vousden, and L. Wade, *Parameter estimation for compact binaries with ground-based gravitational-wave observations using the LALInference software library*, Physical Review D **91**, 10.1103/physrevd.91.042003 (2015).

[10] G. Carullo, W. D. Pozzo, and J. Veitch, *Observational black hole spectroscopy: A time-domain multimode analysis of GW150914*, Physical Review D **99**, 10.1103/physrevd.99.123029 (2019).

[11] C. D. Capano, M. Cabero, J. Westerweck, J. Abedi, S. Kastha, A. H. Nitz, A. B. Nielsen, and B. Krishnan, *Observation of a multimode quasi-normal spectrum from a perturbed black hole* (2021).

[12] M. Isi and W. M. Farr, *maxisi/ringdown: Initial ringdown release* (2021).

[13] E. Berti, J. Cardoso, V. Cardoso, and M. Cavaglià, *Matched filtering and parameter estimation of ringdown waveforms*, Phys. Rev. D **76**, 104044 (2007).

[14] L. C. Stein, *qnm: A Python package for calculating Kerr quasinormal modes, separation constants, and spherical-spheroidal mixing coefficients* (2019).

[15] A. Nitz, I. Harry, D. Brown, C. M. Biwer, J. Willis, T. D. Canton, C. Capano, T. Dent, L. Pekowsky, A. R. Williamson, S. De, M. Cabero, B. Machenschalk, D. Macleod, P. Kumar, F. Pannarale, S. Reyes, G. S. C. Davies, dfinstad, S. Kumar, M. Tápai, L. Singer, S. Khan, S. Fairhurst, A. Nielsen, S. Singh, T. Massinger, K. Chandra, shasvath, and veronica villa, *gwastro/pycbc: v2.0.5 release of PyCBC* (2022).

[16] G. Pratten, C. Garcí a-Quirós, M. Colleoni, A. Ramos-Buades, H. Estellés, M. Mateu-Lucena, R. Jaume, M. Haney, D. Keitel, J. E. Thompson, and S. Husa, *Computationally efficient models for the dominant and subdominant harmonic modes of precessing binary black holes*, Physical Review D **103**, 10.1103/physrevd.103.104056 (2021).

[17] V. Varma, D. Gerosa, L. C. Stein, F. Hébert, and H. Zhang, *High-Accuracy Mass, Spin, and Recoil Predictions of Generic Black-Hole Merger Remnants*, Physical Review Letters **122**, 10.1103/physrevlett.122.011101 (2019).

[18] V. Varma, L. C. Stein, and D. Gerosa, *vijayvarma392/surfinBH: Surrogate Final BH properties* (2018).